

Article

Continuous-Flow Process for Glycerol Conversion to Solketal Using a Brönsted Acid Functionalized Carbon-Based Catalyst

 Vanesa Domínguez-Barroso, Concepción Herrera * , María Ángeles Larrubia, Rafael González-Gil, Marina Cortés-Reyes and Luis J. Alemany *

Departamento de Ingeniería Química, Facultad de Ciencias, Universidad de Málaga, Campus Teatinos s/n, E29071 Málaga, Spain

* Correspondence: concepcionhd@uma.es (C.H.); lujio@uma.es (L.J.A.); Tel.: +34-952-131-919 (L.J.A.)

Received: 17 June 2019; Accepted: 15 July 2019; Published: 18 July 2019

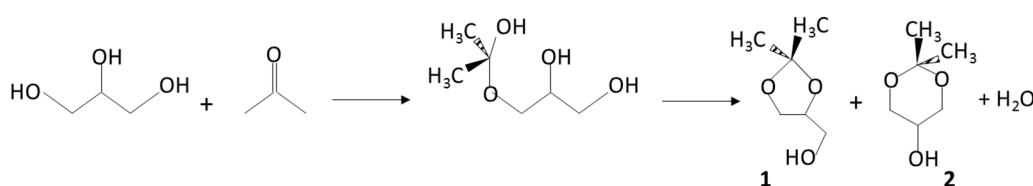


Abstract: The acetalization of glycerol with acetone represents a strategy for its valorization into solketal as a fuel additive component. Thus, acid carbon-based structured catalyst ($\text{SO}_3\text{H-C}$) has been prepared, characterized and tested in this reaction. The structured catalyst ($L = 5 \text{ cm}$, $d = 1 \text{ cm}$) showed a high surface density of acidic sites ($2.9 \text{ mmol H}^+ \text{ g}^{-1}$) and a high surface area. This catalyst is highly active and stable in the solketal reaction production in a batch reactor system and in a continuous downflow reactor, where several parameters were studied such as the variation of time of reaction, temperature, acetone/glycerol molar ratio (A/G) and weight hourly space velocity (WHSV). A complete glycerol conversion and 100% of solketal selectivity were achieved working in the continuous flow reactor equipped with distillation equipment when WHSV is 2.9 h^{-1} , $A/G = 8$ at $57 \text{ }^\circ\text{C}$ in a co-solvent free operation. The catalyst maintained its activity under continuous flow even after 300 min of reaction.

Keywords: biofuel additive; monolithic catalyst; brönsted acidity; glycerol valorization; continuous-flow reactor

1. Introduction

Glycerol excess from biodiesel production provides a good potential raw material for generation of value-added products, such as fuel additives, solvents or chemicals [1–4]. Thus, the strategies for glycerol valorization include a series of very different processes, such as acetalization, hydrogenolysis, esterification, etherification, reforming, pyrolysis or selective oxidation, as has been reported in the literature [5–9]. Glycerol acetalization, in particular, uses glycerol and carbonyl compounds, e.g., aldehydes or ketones yielding cyclic glycerol acetal/ketal molecules. The reaction between acetone and glycerol is presented in Scheme 1, where (1) solketal (2,2-dimethyl-1,3-dioxolane-4-methanol), (2) acetal (1,3-dioxane-5-ol) and water are formed over an acid catalyst [10]. Solketal is used as a solvent, low-temperature heat-transfer fluid, surfactant and as an oxygenated additive to improve biofuel properties, such as cold flow, viscosity, or octane index, as an alternative to commercial trialkylethers (MTBE and ETBE) [11].



Scheme 1. Scheme of reaction of acetalization of glycerol with acetone.

As has been reported in the literature [12], the production of cyclic acetals or ketals is favored in the presence of Brønsted acid catalysts. Traditionally, batch reactors and homogeneous acid catalysts, such as HCl, H₂SO₄, and HF, have been used. More recently, heterogeneous solid acid catalysts such as Amberlyst resins, mixed oxides (niobium-zirconium), functionalized activated carbons and acidic mesoporous silica were proposed in the literature [13–15]. Chem et al. [16] employed heteropolyacids supported on mesoporous silica for acetalization under mild conditions. The main hindrance for acetylation of glycerol to produce solketal is the formation of water, which must be removed to avoid reversibility of reaction and deactivation of heterogeneous catalysts, as described Fehete et al. [17] in their work. Ion exchange resins (amberlyst-15, amberlyst-36, amberlyst-35) show good initial conversion but are prone to fast catalyst deactivation and production of undesirable side products [18,19]. Nevertheless, despite the great potential of the aforesaid catalysts, the production of some of them is costly and a substantial amount of solid catalyst is generally required (5–40%), being too expensive to be applied in the large-scale production and in many cases, complete conversion of glycerol is rarely achieved [20].

Operational aspects of the reaction of glycerol with acetone include a wide range of temperatures from room temperature to acetone boiling point, in which case, the removal of water is desirable in order to shift the equilibrium to the products through a reactive distillation process [21]. Acetone/glycerol ratio is another parameter to be taken into account and a range from 2/1 to 8/1 was used. The utilization of a cosolvent, due to the limited miscibility of these compounds at the start of the reaction [22] is also considered. Besides, the removal of water from the reaction mixture is useful to shift the equilibrium of the reaction, in this way, petroleum ethers or chloroform can be used [23].

Up to now, most investigations have been performed in a batch reactor and the large-scale production would present certain advantages, but some process improvements are necessary in terms of costs, catalysts, and efficiency. Recently, Shirani et al. [24] examined an easy-to-scale up continuous system using a heterogeneous catalyst as purolite PD206 catalyst for efficient conversion of glycerol to solketal (95% of yield), at higher residence time under the following reaction conditions of temperature, pressure, feed flow rate, and catalyst's mass: 20 °C, 120 bar, 0.1 mL min⁻¹ and 0.77 g, respectively. Nanda et al. [14] developed an efficient continuous flow process employing several heterogeneous catalysts and, in particular, using a strongly acidic amberlyst, a maximum solketal yield was achieved at 40 °C, 600 psi and weight hourly space velocity (WHSV) of 4 h⁻¹.

In the present work, a monolithic structured carbon-based support functionalized with sulfonic acid was prepared from cellulose, characterized and tested in the reaction of glycerol acetalization. The effect of reaction conditions (acetone/glycerol molar ratio, temperature, time of reaction and weight hourly space velocity, WHSV) was studied in a batch reactor and in a down-flow continuous reactor as the first approach to scale up the process.

2. Results and Discussion

2.1. Carbon-Based Support and Catalyst Characterization

A methodology was established to prepare a biogenic conformed carbonaceous support starting from spiral-wound laminated cellulose, considering several steps: Pyrolysis at different temperatures (400–800 °C) and chemical activation (HNO₃). Finally, the catalyst was obtained after acid functionalization, giving a monolithic structured SO₃H-C catalyst (L = 5 cm and d = 1 cm). After these synthesis steps, the materials were characterized.

Scanning electron microscopy images (SEM) of the cellulose treated in N₂ flow at different temperatures (600 and 800 °C) are shown in Figure 1. SEM images show a very similar morphology, regardless of the pyrolysis temperature. This implies that the range of temperature utilized in this procedure is not a relevant factor affecting the morphology of the material. The typical morphology of cellulose fibers is observed [25], where many long fibers with thicknesses of 5–30 μm were aggregated and the dependence on the average thickness of the fibrils with those of the original material without

any treatment is denoted. Additionally, it can be observed in the magnified SEM images in Figure 1c,d that each fiber is composed of many thinner fibrils, having nanometric diameters.

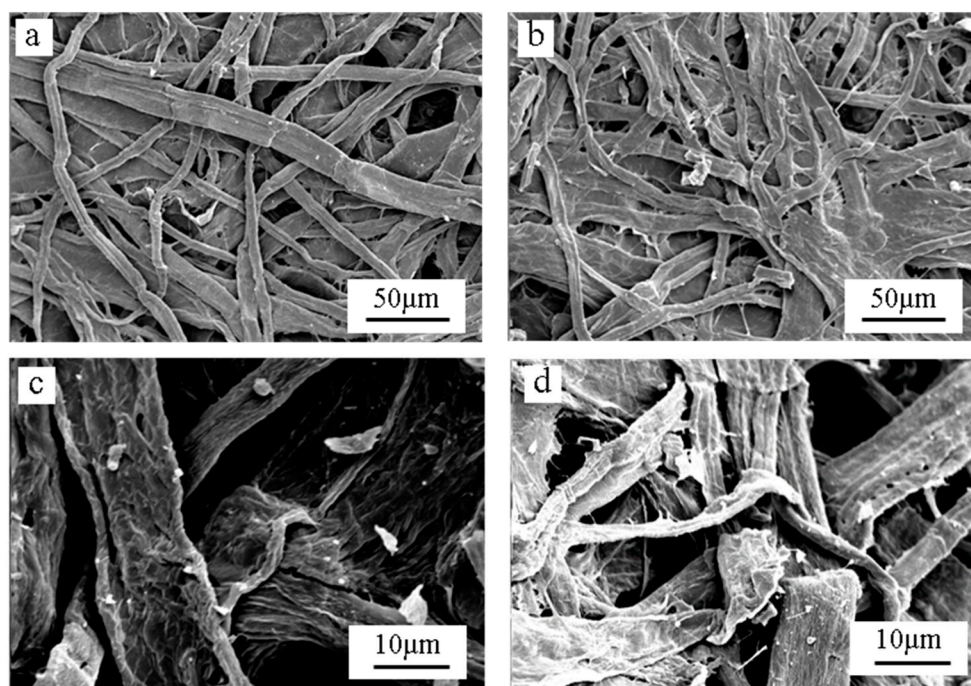


Figure 1. SEM images of the carbonaceous material obtained by cellulose pyrolysis at 600 °C (a) and 800 °C (b) and magnified SEM images (c,d).

Figure 2 depicts Raman spectra of the cellulose treated in N₂ flow at different temperatures. Raman profiles were very similar, and the two strong and broad bands, attributed to the disordered structure (D-band, ~1350 cm⁻¹) and the crystalline sp² hexagonal carbon band network (G-band, ~1580 cm⁻¹) are observed [26]. The intensity of these two signals is dependent on the temperature treatment and becomes sharper with increasing heat-treatment temperature and their position is slightly shifted.

From the Raman spectra, the integrated intensity ratio of these two signals, D and G, is related to graphite crystallite size (L_n) according to [27]:

$$L_n(\text{nm}) = \frac{4.4}{R} \text{ where } R = \frac{I_D}{I_G} \quad (1)$$

Considering that both signals have similar extinction coefficients, it is possible to calculate the graphitic fraction as follows:

$$X_G = \frac{I_G}{I_G + I_D} \text{ or } \frac{1}{1 + R} \quad (2)$$

These calculated values are listed in Table 1. The intensity ratio of D and G signals denoted by $R = I_D/I_G$, decreases with increasing the temperature of pyrolysis what implies the increase of the graphitic fraction in the fibers and X_G , are 0.181, 0.350 and 0.408 at 400 °C, 600 °C and 800 °C, respectively. The graphite crystallite size, L_n , was estimated to be 0.98, 2.37, and 3.03 at 400 °C, 600 °C, and 80 °C, respectively.

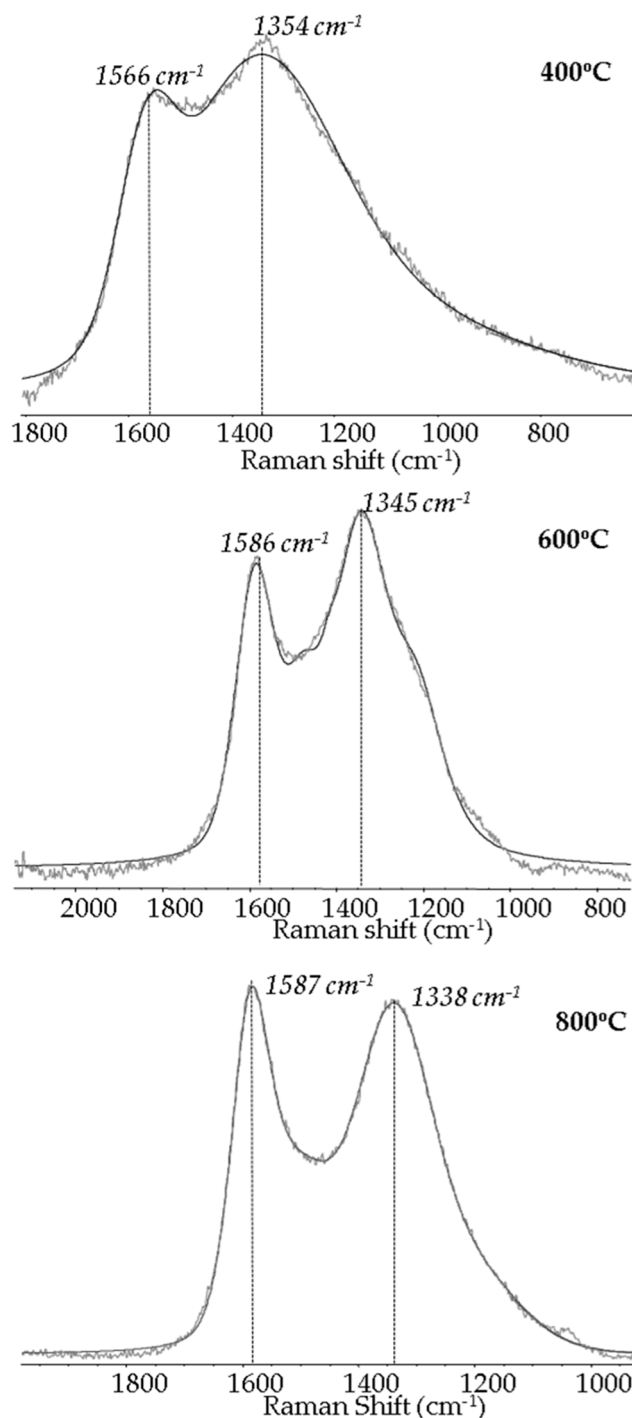


Figure 2. Raman spectra of the carbonaceous material obtained by pyrolysis at 400 °C, 600 °C, 800 °C. Raman condition (532 nm, 10 mW).

There is a clear presence of graphitic and non-graphitic carbon in the support and, with the exception of that pyrolyzed at 400 °C that seems to be insufficient for the pyrolyzation process, there is minor difference in which graphitization occurs between 600 °C and 800 °C. Therefore, 600 °C was the temperature chosen for the first step of pyrolysis of cellulose. The BET surface area of the cellulose pyrolyzed at 600 °C was 19 m² g⁻¹ (57% related to microporosity) and the total pore volume was 0.058 cm³ g⁻¹. The BET surface of the cellulose pyrolyzed at 800 °C was 25 m² g⁻¹ and the total pore volume was 0.035 cm³ g⁻¹.

Table 1. Raman, XPS and Elemental Analysis of the material after the different step of synthesis.

Raman Data ^a	Temperature of Pyrolysis (°C)						
	400 °C	600 °C	800 °C				
D peak position (cm ⁻¹)	1354	1345	1338				
G peak position (cm ⁻¹)	1566	1586	1587				
R = I _D /I _G	4.501	1.859	1.453				
L _n = 4.4 nm/R	0.98	2.37	3.03				
x _G = 1/(1 + R)	0.181	0.350	0.408				
XPS Data	Relative Amount (%)				Atomic Ratio	Deconvolution of C _{1s} and O _{1s}	
	C _{1s}	O _{1s}	N _{1s}	S _{2p}	O/C	C _{1s}	O _{1s}
C support ^b	94.78	5.22	n.d.	-	0.06	284.8 (78)	532.9 (100)
						286.4 (15)	-
C support ^c	80.00	17.10	2.82	-	0.21	284.7 (65)	532.0 (47)
						286.2 (29)	534.1 (53)
						288.9 (6)	
Elemental Analysis	Composition (%)			Ratio (%)			
	C	N	H	S	O	O/C	
C support ^b	95.15	n.d.	0	-	4.68	0.05	
C support ^c	78.27	2.32	7.58	-	11.67	0.15	

^a cellulose pyrolysis, ^b pyrolyzed at 600 °C, ^c pyrolyzed at 600 °C and chemically activated with HNO₃, n.d. non detected.

The carbonaceous support was then chemically activated with HNO₃ (3N) at room temperature for 24 h and after that, treated in inert atmosphere at 300 °C. In Table 1, the characterization results are listed. From XPS, the overall concentration of oxygen has increased, and after HNO₃ activation, a higher O/C ratio of 0.21 was obtained.

Moreover, the deconvolution of O1s bands after the nitric treatment reveals the presence of different peaks that are assigned to carbonylic groups (c.a. 532.0 eV) and carboxylic groups (c.a. 534.1 eV) [28]. Regarding the relative amount of each oxygen-bonded species, nitric oxidation treatment increases the percentage of oxygen from carboxylic groups (53%). As was described in [29], C1s peak has been fitted into different contributions: Graphitic carbon (ca. 284.8 eV) with a variable relative percentage before and after chemical activation (78–65%), carbonylic (ca. 286 eV), and carboxylic groups (ca. 288–289 eV) [28].

The O/C atomic ratios obtained from elemental analysis are similar to those estimated as atomic surface ratio registered by XPS, which suggests some bulk uniformity. In fact, an increase of 3.5 times in the O/C ratio was observed for the carbonaceous support after chemical activation in comparison with the pyrolyzed material. Nitrogen is also present in the samples after nitric acid treatment due to the low-temperature treatment (300 °C).

Finally, the carbonaceous support (pyrolyzed at 600 °C and treated with HNO₃) was functionalized with sulfonic groups by the impregnation technique and characterized. It was labeled as SO₃H-C. In the TEM image (Figure 3) a surface typical of carbonized materials is observed as was reported by other authors [30]. EDX microanalysis clearly showed the presence of well-dispersed sulfur after the sulfonic treatment, as well as oxygen and carbon in the catalyst surface.

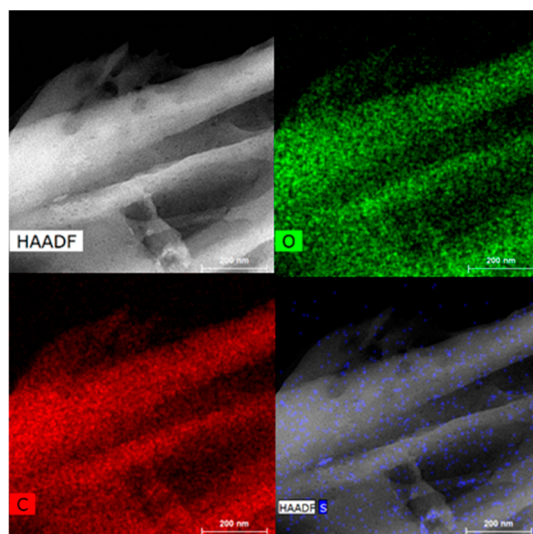


Figure 3. TEM images of the SO₃H-C catalyst.

A summary of the characterization results is listed in Table 2 for the functionalized sulfonic-acid carbon catalyst (SO₃H-C). Although the graphitic fraction is kept constant and close to 0.31, the BET area and pore volume increased up to 384 m² g⁻¹ and 0.16 cm³ g⁻¹, respectively. This can be in part associated with the chemical activation treatment to which the support was undergone and although to a lesser extent, to the incorporation of sulfonic acid precursor employed and successive thermal treatment for stabilizing the catalyst.

Table 2. Characterization results of SO₃H-C catalyst. Raman, XPS and elemental analysis.

Raman Data	Peak Position (cm ⁻¹)		R = I _D /I _G	La = 4.4 nm/R	X _G = 1/(1 + R)				
	D	1338	2.26	1.95	0.31				
	G	1589							
XPS Data	Relative Amount (%)				Atomic Ratio	Deconvolution of C _{1s} O _{1s} and S _{2p}			
	C _{1s}	O _{1s}	N _{1s}	S _{2p}	O/C	C _{1s}	O _{1s}	S _{2p}	
	62.42	30.55	1.39	5.65	0.50	284.7 (65)	532.0 (55)	169.5 (100)	
						286.2 (29)	533.4 (40)		
						288.9 (6)	534.6 (6)		
Elemental Analysis	Composition (%)					Ratio (%)		Acid Density (mmol H ⁺ g ⁻¹)	
	C	O	H	S	N	O/C	S/C		
	51.9	38.51	3.82	4.51	1.17	0.61	0.12	1.54 ^a	2.93 ^b

^a calculated from elemental analysis, ^b calculated by titration.

From XPS data, it was estimated an O/C atomic ratio close to 0.5, slightly lower than that registered from elemental analysis (O/C = 0.61) and corresponds with a sulfo-oxygenated group enriched expose surface. S_{2p} signal at 169 eV is associated with the presence of sulfur (+6) species only related to sulfonic species [31].

O_{1s} and C_{1s} signals have been deconvoluted and, in comparison with the support after chemical activation, no differences are observed in the relative amount of surface species relative to the deconvolution of the C_{1s} signal. However, for the O_{1s} signal, the relative percentages of the detected signals differ since at 532.0 eV the signals of carbonylic groups overlapped with one of sulfonic groups [32], giving a higher value of 55% and a decrease in the signal relative to the carboxyl groups at 533.4 eV (40%), another contribution at higher binding energy can be associated with some hydroxyls groups generated after functionalization. N_{1s} signal presented a band at binding energy close to 400 eV, that can be associated to C-N groups [33], besides, due to its asymmetry. Another contribution

can be envisaged due to residual nitrate groups, maintained after sulfonic functionalization and thermal treatment (in N_2 at $300\text{ }^\circ\text{C}$). The contribution of the C-N group in the signal relative to the C1s ($284\text{--}286\text{ eV}$) cannot be ruled out, but nevertheless it is not easily detectable due to the proximity in binding energy with those that present the carbonyls and carboxyls groups, which are the majority. This contribution is not appreciable in the infrared spectrum of the catalyst and, therefore, a precise assignation cannot be performed.

The acid site density of the catalyst was determined by elemental analysis as was proposed by Hara et al. [34]. As every sulfur atom present in the catalyst exists as $-\text{SO}_3\text{H}$, as was determined by XPS, the sulfur content obtained from elemental analysis was used to calculate the sulfonic acid density, as its protonated form as Brönsted acid sites. The acid site density calculated by this method was of 1.5 mmol g^{-1} and besides, the acidity was also calculated by Boehm titration [35] with aqueous solutions of NaOH, giving a value of 2.9 mmol g^{-1} , higher value masked by residual population of surface carboxylic groups associated with the carbon-support.

FT-IR spectrum of $\text{SO}_3\text{H-C}$ catalyst is presented in Figure 4. Absorption bands of sulfonic acid are recorded at 1285 , 1177 , 1070 and 614 cm^{-1} which correspond to the asymmetric and symmetric $\text{O}=\text{S}=\text{O}$ and S-O stretching vibration of the sulfonic group (SO_3H), respectively [28,36]. Therefore, the presence of sulfur as sulfonic groups is confirmed without bands associated with sulfate groups, which can easily be leached in the reaction conditions, as was observed for other catalyst based on mixed oxides. Another signal at 620 cm^{-1} is related to the bending vibration of $-\text{OH}$ groups hydrogen bonded to $-\text{SOH}$.

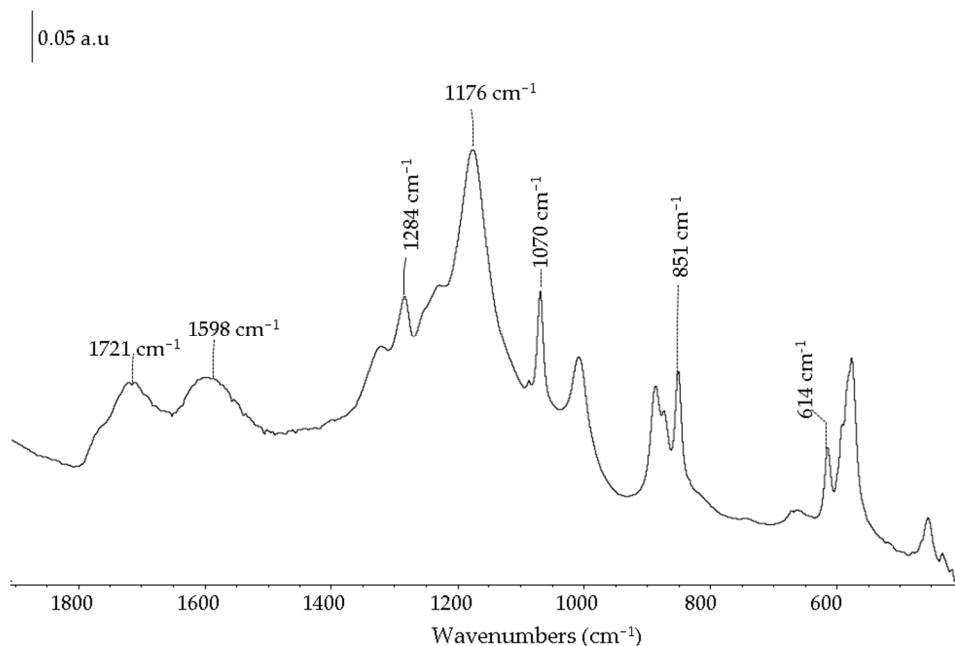


Figure 4. FTIR in KBr disc of the $\text{SO}_3\text{H-C}$ catalyst.

The vibration bands observed at 1620 and 1720 cm^{-1} are due to aromatic $\text{C}=\text{C}$ and $\text{C}=\text{O}$ from different functional groups as carboxyls and carbonyls [37,38]. All these observations confirm the functionalization of the carbonaceous support surface.

2.2. Catalytic Test

2.2.1. Batch-Reactor Experiments

The catalyst, $\text{SO}_3\text{H-C}$, was tested in the acetalization reaction of glycerol in a batch reactor (500 mL, 10% wt. of catalyst) in which several microliths of catalyst were loaded into the catalyst holder basket as will be described in the experimental section.

The influence of several parameters, such as time of reaction (0.5–60 min), acetone to glycerol molar ratio ($A/G = 1/1$ – $8/1$) and reaction temperature ($30\text{ }^{\circ}\text{C}$ and reflux temperature of acetone), has been evaluated. Figure 5 presents the conversion of glycerol in function of acetone/glycerol molar ratio at a different time of reaction, 15, 30, and 60 min (Figure 5a). As it can be observed, the conversion is highly dependent of A/G ratio due to the fact that an excess of acetone increases the poor solubility of the reactants [23]. Additionally, by increasing the acetone glycerol molar ratio, the reaction could drive itself forward, favoring solketal production [39] and increases at increasing A/G ratio, so a maximum equilibrium conversion of 80% is achieved at $A/G = 8/1$. For a fixed A/G ratio, higher time of reaction achieved higher conversion rates, so values of 40%, 60%, and 70% are obtained at A/G of 2/1, 4/1 and 6/1 respectively for 60 min of reaction.

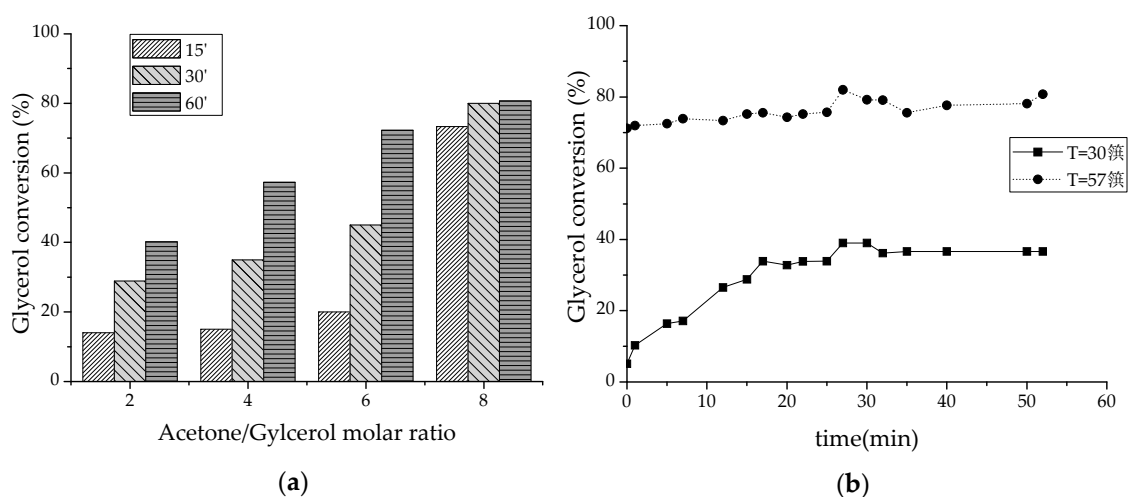


Figure 5. (a) Glycerol conversion vs. A/G molar ratio in batch reactor for 15, 30, and 60 min of reaction and (b) glycerol conversion vs. time at different reaction temperature ($A/G = 8/1$).

At $30\text{ }^{\circ}\text{C}$, glycerol conversion increases with time of reaction up to a limited value of 40%, and working at the reflux acetone temperature ($57\text{ }^{\circ}\text{C}$), the equilibrium conversion was near 80%, maintained with the time of reaction.

In Figure 6, FTIR spectra of the reaction product evolution with time are shown ($A/G = 8/1$, $57\text{ }^{\circ}\text{C}$). At the start of the reaction, t_0 , the spectrum presents bands overlapped due to acetone and glycerol. Therefore, the three signals centered at 1100 , 1042 and 993 cm^{-1} are associated with the triol structure of glycerol. At 1714 cm^{-1} and 1373 cm^{-1} the modes are associated with the $\text{C}=\text{O}$ bond and to methyl groups of acetone, respectively. At higher wavenumbers, a wideband is observed between 3400 and 3600 cm^{-1} associated with hydroxyl groups and those related to methyl groups at 2938 – 2884 cm^{-1} are also present. After 15 min of reaction, a decrease in the bands related to glycerol is observed and bands at around 1157 cm^{-1} and 1114 cm^{-1} can be attributed to the symmetrical stretching of $\text{C}-\text{O}$ band, and the signals observed at 1216 cm^{-1} and at 1047 cm^{-1} , characteristic of the $\text{C}-\text{O}$ bonds of the five-membered ring, in agreement with the reported by Nanda et al. [14]. The strong and wide band at around 3400 – 3600 cm^{-1} was also observed and it is ascribed to $\text{O}-\text{H}$ stretching band resulted in the intermolecular and intramolecular hydrogen bonds present in solketal, whereas the signals localized at 2987 cm^{-1} and 2884 cm^{-1} refers to the formation bands and asymmetric axial deformation of the $\text{C}-\text{H}$ bands of the methyl groups. GC-MS analysis confirms a solketal selectivity higher than 99%, without the six-member ring acetal as a byproduct [40].

Therefore, the prepared monolithic Brönsted acid catalyst, $\text{SO}_3\text{H}-\text{C}$, is active and highly selective to solketal achieving 80% of conversion at high A/G and working at a temperature near acetone boiling point and batch reactor mode operation.

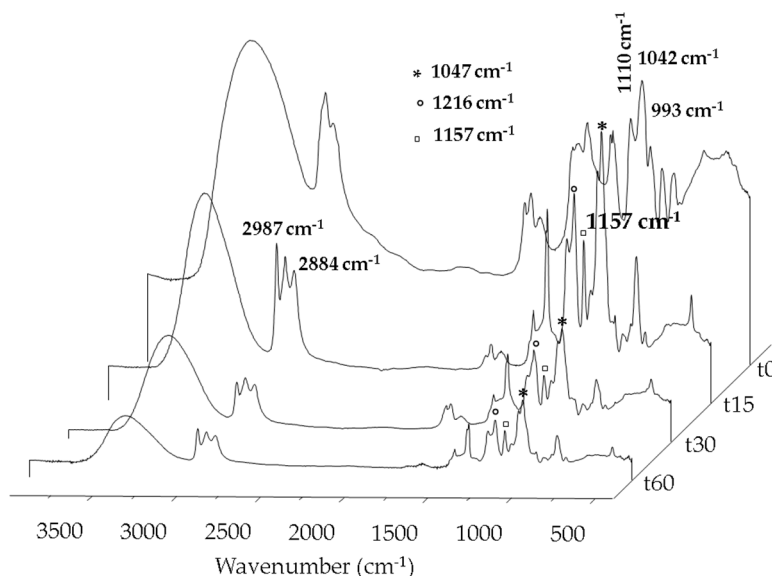


Figure 6. FTIR spectra of the reaction product (A/G = 8/1, 57 °C) at a different time of reaction.

2.2.2. Continuous-Flow Reactor Experiments

The monolithic structured catalyst ($\text{SO}_3\text{H-C}$, $L = 5$ cm and $d = 1$ cm) was tested in a laboratory scale continuous down-flow reactor (1.5 cm ID and 10 cm length) coupled to a distillation equipment. The reactants were pumped and mixed into the reactor, filled with the monolithic catalyst and small glasses spheres, acting as premixing chamber. The effect of WHSV was studied at a reflux temperature of acetone and acetone/glycerol molar ratio close to 8. In Figure 7a, the conversion of glycerol and the selectivity to solketal are plotted versus WHSV. At 2.9 h^{-1} , complete glycerol conversion is detected. However, by increasing WHSV, glycerol conversion decreases to a value of 92% at 8.9 h^{-1} , since shorter residence times (or larger WHSV) lead to lower equilibrium conversion [41]. For all experiments, the selectivity is 99% for solketal. In comparison with the published by other authors working in continuous flow reaction and solid acid catalyst, Shirani et al. [24] reported a 64% of glycerol conversion using acetone/glycerol molar ratio of 8/1, 57 °C and a cosolvent. Other authors informed about the need for high pressure to improve the acetone/glycerol solubility.

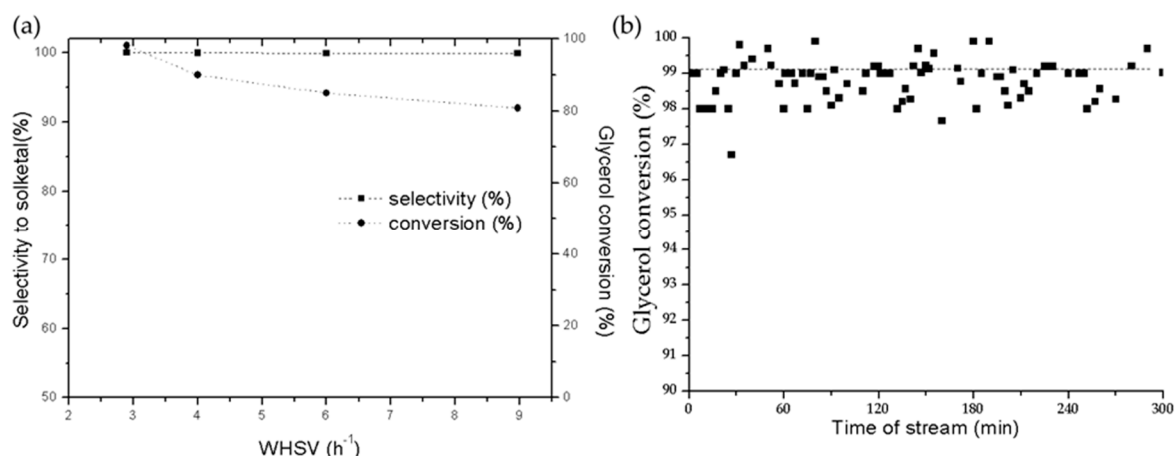


Figure 7. (a) Solketal selectivity and glycerol conversion vs. WHSV (b) Glycerol conversion vs. time of reaction (A/G = 8/1, 57 °C, WHSV = 2.9 h^{-1}).

The conversion of glycerol was also evaluated after 300 min of reaction (A/G = 8/1, 57 °C, WHSV = 2.9 h^{-1}) and the results are showed in Figure 7b. As it can be observed, the catalyst maintained its activity, moreover, neither leaching of the Brönsted acid sites associated with sulfonic groups nor sulfur

species were detected in the liquid product, as was checked after the reaction. Another important factor is the interaction of the catalyst with the water generated in the reaction, since one mole of water is formed per mole of solketal, which would lead to a decrease in the activity. So, due to the characteristic of the catalyst and, more specifically, the carbon-based support seems to possess a key hydrophobic character since it did not deteriorate its textural properties and acid sites density after reactivity tests.

This study suggests that the SOH₃-C catalyst is highly active and selective under glycerol/acetone acetalization reaction even under continuous flow operation mode without external pressure or co-solvents. No loss of its morphological characteristics or catalytic properties and no leaching of the Brønsted acid functional groups were observed.

3. Materials and Methods

The biomass used to produce the carbonaceous support of the catalyst was cellulose purchased from Sigma-Aldrich. Nitric acid (65%) and methanesulfonic acid (99.5%) were supplied by Sigma-Aldrich. Glycerol and acetone with a purity of 99.5% were used.

3.1. Catalyst Preparation and Characterization

Structured biomorphic carbon based-catalyst was prepared within the following steps: First, a spiral-wound laminated cellulose ($L = 5$ cm and $d = 1$ cm) was pyrolyzed under a continuous flow of nitrogen for 2 h between 400 and 800 °C and at a heating rate of 10 °C min⁻¹. Then, it was chemically activated by oxidation treatment with HNO₃ (3M) under stirring during 24 h at room temperature after that, it was dried and treated at 300 °C in nitrogen atmosphere. Then, acidic sites as sulfonic (SO₃H) groups were incorporated to the carbon-based activated support by impregnating it with a methanesulfonic acid solution with SO₃H (specific volume of cellulose: 2 mL g⁻¹). The SO₃H content expressed as weight percentage with respect the weight support was of 5% w/w. Finally, the material was thermally treated under a nitrogen atmosphere at 300 °C for 2 h and at a heating rate of 10 °C min⁻¹.

The support and the final catalyst were characterized using several techniques. SEM micrographs were obtained with a scanning electron microscope JEOL JSM-840. Prior to recording the images, a fine gold layer was sprayed on the sample to assure conduction. The porous structures of the samples were characterized by adsorption/desorption of N₂ at 77 K using a Micromeritics ASAP 2020. The specific surface area was obtained by the BET isotherm equation and the pore volume by the Barrett-Joyner-Halenda (BJH) method from the desorption branch of the isotherm. A Talos F200X instrument from FEI was used for the high resolution TEM images and EDX mapping. X-ray photoelectron spectra were recorded on a physical electronic 5701 spectrometer equipped with a PHI 10-360 analyzer using the MgKα X-ray source. Binding energy (BE) values were referred to the C1s signal (284.8 eV) from the adventitious carbon. Deconvolution of experimental curves was done with Gaussian and Lorentzian line fitting, minimizing the χ^2 values. Raman spectra were recorded in a DXR Raman microscope (Thermo Scientific) working at $\lambda = 532$ nm and 10 mW and incorporating a CCD detector charge couple device. FT-IR spectra in the wavelength range of 4000–400 cm⁻¹ were obtained using an Avatar 6700 Thermo Electronic Corporation equipment. Elemental analysis was performed using a Perkin-Elmer 2400 analyzer. Acidic character was measured by titration according to [35].

3.2. Catalytic Tests

Glycerol reaction with acetone was firstly approached under batch conditions in a jacket heated reactor of 500 mL and at atmospheric pressure. The system was externally heated by a water bath and fitted with a mechanical stirrer, a thermocouple for temperature control and a reflux condenser. For each experiment, fresh catalyst consisting of several monoliths of $L = 1$ cm and $d = 0.5$ cm (10% w/w respect to the glycerol feed, $\rho_{ap} = 0.30$ g cm⁻³) were loaded into the reactor, placed in a basket that rotates on a shaft, see Figure 8 (left), and the stirring rate was set at 250 rpm. The effect of molar ratio of A/G (2/1–8/1), temperature (between room temperature and reflux temperature of acetone) and time of reaction (from 0 to 60 min) was evaluated.

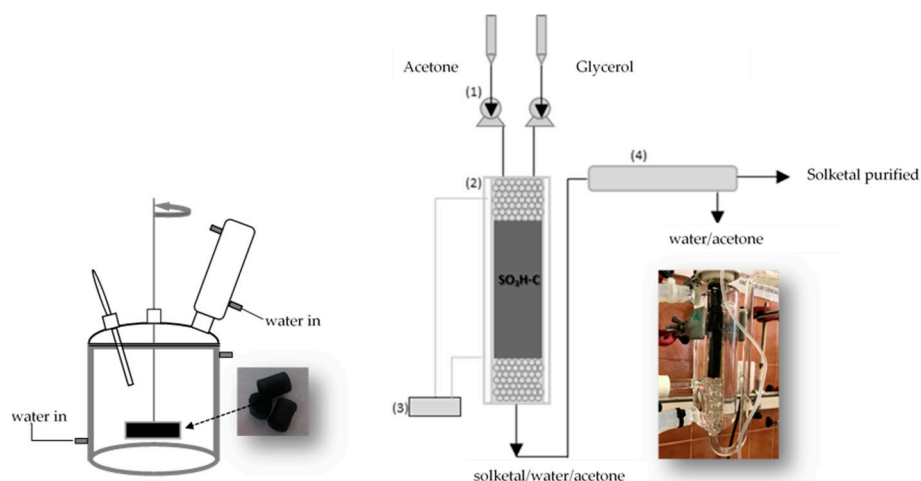


Figure 8. Batch reactor system (on the left) and continuous flow reactor system (on the right), (1) feed pump (2) tubular reactor (3) thermostatic water bath control (4) distillation equipment.

Glycerol reaction was also carried out in a laboratory scale continuous down-flow reactor (1.5 cm ID and 10 cm length) heated with an external water bath connected to a thermostat and coupled to distillation equipment. A schematic diagram of this reaction system is shown in Figure 8 (right). The feed, glycerol, and acetone at a selected molar ratio were pumped at a specific flow rate into the reactor maintained at a desired temperature (controlled by a water bath). In a typical run, 2.05 mL h⁻¹ of acetone and 2.5 mL h⁻¹ of glycerol were mixed into the reactor corresponding to 8:1 molar ratio acetone:glycerol. The monolithic catalyst (L = 5 cm and d = 1 cm) was loaded into the reactor filled with some glass spheres, which was used as an initial pre-mixer. Weight hourly space velocity, WHSV (as mass flow of glycerol per gram of catalyst) was varied from 2.9 to 8.9 h⁻¹. After the reaction, the liquid phase separated into acetone, water, and solketal was weighed and analyzed by gas chromatograph-mass spectrometer using a DSQ from Thermo Scientific equipped with a column ZB-5 (30 m × 0.25 mm (ID) × 0.25 micras thickness) and by FTIR using an Avatar 6700 from Thermo Electronic Corporation.

Glycerol conversion, solketal yield, and product selectivity were calculated as follows:

$$\text{Yield (\%)} = \frac{F_S}{I_G} \times 100 \quad (3)$$

$$\text{Glycerol conversion (\%)} = \frac{I_G - F_G}{I_G} \times 100 \quad (4)$$

$$\text{Selectivity (\%)} = \frac{F_S}{I_G - F_G} \times 100 \quad (5)$$

where I_G is the initial mole of glycerol, F_G is the final mole of glycerol and F_S is the final mole of solketal formed obtained by gravimetry.

4. Conclusions

A Brönsted acid sulfonic carbon-based catalyst structured in the form of monolith was obtained. A methodological procedure was established to obtain the catalyst through different steps of pyrolysis, chemical activation, and acidic functionalization. It showed a high BET area and an acidic density sites of 2.9 mmol H⁺ g⁻¹ and presented high performance and stability in the acetalization reaction of glycerol working under continuous flow reaction conditions, at high A/G ratio, reflux acetone temperature, without leaching or losing activity even under long reaction time and water formation in the reaction products, yielding the five member ring, solketal.

Author Contributions: Experiment, V.D.B, R.G.G and M.C.R; Data Curation, V.D.B, C.H. and L.J.A; Writing–Original Draft Preparation, V.D.B and C.H; Writing–Review & Editing, M.A.L., C.H and V.D.B; Supervision, C.H., M.A.L and L.J.A; Project Administration, L.J.A. and C.H.; Funding Acquisition, M.A.L., C.H. and L.J.A.

Funding: Authors want to thank the financial support of CTQ 2017-87909R project.

Conflicts of Interest: The authors declare no conflicts of interest.

References

1. Smirnov, A.A.; Selishcheva, S.A.; Yakovlev, V.A. Acetalization catalysts for synthesis of valuable oxygenated fuel additives from glycerol. *Catalysts* **2018**, *8*, 598. [[CrossRef](#)]
2. Ayoub, M.; Abdullah, A.Z. Critical review on the current scenario and significance of crude glycerol resulting from biodiesel industry towards more sustainable renewable energy industry. *Renew. Sustain. Energy Rev.* **2012**, *16*, 2671–2686. [[CrossRef](#)]
3. Gu, Y.; Jerome, F. Glycerol as a sustainable solvent for green chemistry. *Green Chem.* **2010**, *12*, 1127–1138. [[CrossRef](#)]
4. Garcia, E.; Laca, M.; Perez, E.; Garrido, A.; Peinado, J. New class of acetal derived from glycerine as a biodiesel fuel component. *Energy Fuels* **2008**, *22*, 4274–4280. [[CrossRef](#)]
5. Ntumba Tshibalonza, N.; Monbaliu, J.C.M. Revisiting the deoxydehydration of glycerol towards allyl alcohol under continuous-flow conditions. *Green Chem.* **2017**, *19*, 3006–3013. [[CrossRef](#)]
6. Moreira, A.B.F.; Bruno, A.M.; Souza, M.M.V.M.; Manfro, R.L. Continuous production of lactic acid from glycerol in alkaline medium using supported copper catalysts. *Fuel Process. Technol.* **2016**, *144*, 170–180. [[CrossRef](#)]
7. Bruno, A.M.; Chagas, C.A.; Souza, M.M.V.M.; Manfro, R.L. Lactic acid production from glycerol in alkaline medium using Pt-based catalysts in continuous flow reaction system. *Renew. Energy* **2018**, *118*, 160–171. [[CrossRef](#)]
8. Rastegari, H.; Ghaziaskar, H.S.; Yalpani, M.; Shafiei, A. Development of a continuous system based on azeotropic reactive distillation to enhance triacetin selectivity in glycerol esterification with acetic acid. *Energy Fuels* **2017**, *31*, 8256–8262. [[CrossRef](#)]
9. Calmanti, R.; Galvan, M.; Amadi, E.; Perosa, A.; Selva, M. High-temperature batch and continuous-flow transesterification of alkyl and enol esters with glycerol and its acetal derivatives. *ACS Sustain. Chem. Eng.* **2018**, *6*, 3964–3973. [[CrossRef](#)]
10. Li, Z.; Miao, Z.; Wang, X.; Zhao, J.; Zhou, J.; Si, W.; Zhuo, S. One-pot synthesis of ZrMo-KIT-6 solid acid catalyst for solvent-free conversion of glycerol to solketal. *Fuel* **2018**, *233*, 377–387. [[CrossRef](#)]
11. Samoilov, L.; Maximov, V.O.; Stolonogova, T.I.; Chernysheva, E.A.; KapustinbA, O.K.; Arpunina, V.M. Glycerol to renewable fuel oxygenates. Part I: Comparison between solketal and its methyl ether. *Fuel* **2019**, *249*, 486–495. [[CrossRef](#)]
12. Mallesham, B.; Sudarsanam, P.; Raju, G.; Reddy, B.M. Design of highly efficient Mo and W promoted SnO₂ solid acids for heterogeneous catalysis: Acetalization of bioglycerol. *Green Chem.* **2013**, *15*, 478–489. [[CrossRef](#)]
13. Pinto, B.P.; De Lyra, J.T.; Nascimento, J.A.C.; Mota, C.J.A. Ethers of glycerol and ethanol as bioadditives for biodiesel. *Fuel* **2016**, *168*, 76–80. [[CrossRef](#)]
14. Nanda, M.R.; Yuan, Z.; Qin, W.; Ghaziaskar, H.S.; Poirier, M.-A.; Xu, C.C. A new continuous-flow process for catalytic conversion of glycerol to oxygenated fuel additive: Catalyst screening. *Appl. Energy* **2014**, *123*, 75–81. [[CrossRef](#)]
15. Roldan, L.; Mallada, R.; Fraile, J.M.; Mayoral, J.A.; Menendez, M. Glycerol upgrading by ketalization in a zeolite membrane reactor. *Asia-Pac J Chem. Eng.* **2009**, *4*, 279–284. [[CrossRef](#)]
16. Chen, L.; Nohair, B.; Zhao, D.; Kaliaguine, S. Glycerol acetalization with formaldehyde using heteropolyacid salts supported on mesostructured silica. *Appl. Catal. A Gen.* **2018**, *549*, 207–215. [[CrossRef](#)]
17. Fechete, I.; Wang, Y.; Védrine, J.C. The past, present and future of heterogeneous catalysis. *Catal. Today* **2012**, *189*, 2–27. [[CrossRef](#)]
18. Wang, Z.Q.; Zhang, Z.; Yu, W.J.; Li, L.D.; Zhang, M.H.; Zhang, Z.B. A swelling-changeable catalyst for glycerol acetylation with controlled acid concentration. *Fuel Process. Technol.* **2016**, *142*, 228–234. [[CrossRef](#)]

19. Zhou, L.; Nguyen, T.-H.; Adesina, A.A. The acetylation of glycerol over amberlyst-15: Kinetic and product distribution. *Fuel Process. Technol.* **2012**, *104*, 310–318. [[CrossRef](#)]
20. Nda-Umar, U.I.; Ramli, I.; Taufiq-Yap, Y.H.; Muhamad, E.N. An overview of recent research in the conversion of glycerol into biofuels, fuel additives and other Bio-Based chemicals. *Catalysts* **2019**, *5*, 15. [[CrossRef](#)]
21. Reddy, P.S.; Sudarsanam, P.; Malleshham, B.; Raju, G.; Reddy, B.M. Acetalisation of glycerol with acetone over zirconia and promoted zirconia catalysts under mild reaction conditions. *J. Ind. Eng. Chem.* **2011**, *17*, 377–381. [[CrossRef](#)]
22. Esteban, J.; Vorholt, A.J.; Behr, A.; Ladero, M.; Garcia-Ochoa, F.J. Liquid–Liquid Equilibria for the System Acetone + Solketal + Glycerol at (303.2, 313.2, and 323.2) K. *Chem. Eng. Data.* **2014**, *59*, 2850–2855. [[CrossRef](#)]
23. Nanda, M.R.; Zhang, Y.; Yuan, Z.; Qin, W.; Ghaziaskar, H.S.; Xu, C. Catalytic conversion of glycerol for sustainable production of solketal as a fuel additive: A review. *Renew. Sustain. Energy Rev.* **2016**, *56*, 1022–1031. [[CrossRef](#)]
24. Shirani, M.; Ghaziaskar, H.S.; Xu, C. Optimization of glycerol ketalization to produce solketal as biodiesel additive in a continuous reactor with subcritical acetone using Purolite®PD206 as catalyst. *Fuel Process. Technol.* **2014**, *124*, 206–211. [[CrossRef](#)]
25. Krishnamachari, P.; Hashaikh, R.; Materials, M.T. Modified cellulose morphologies and its composites; SEM and TEM analysis. *Micron* **2011**, *42*, 751–761. [[CrossRef](#)]
26. Wang, Y.; Serrano, S.; Avilés, J.J. Raman characterization of carbon nanofibers prepared using Electrospinning. *Synth. Met.* **2003**, *138*, 423–427. [[CrossRef](#)]
27. Ulla, M.A.; Valera, A.; Ubieto, T.; Latorre, N.; Romeo, E.; Milt, V.G.; Monzón, A. Carbon nanofiber growth onto a cordierite monolith coated with Co-mordenite. *Catal. Today* **2008**, *133–135*, 7–12. [[CrossRef](#)]
28. Boyano, A.; Herrera, C.; Larrubia, M.A.; Alemany, L.J.; Moliner, R.; Lázaro, M.J. Vanadium loaded carbon-based monoliths for the on-board no reduction: Influence of temperature and period of the oxidation treatment. *Chem. Eng. J.* **2010**, *160*, 623–633. [[CrossRef](#)]
29. Sadezky, A.; Muckenhuber, H.; Grothe, H.; Niessner, R.; Pöschl, U. Raman microspectroscopy of soot and related carbonaceous materials: Spectral analysis and structural information. *Carbon* **2005**, *43*, 1731–1742. [[CrossRef](#)]
30. Ma, L.; Zhang, X.; Lin, D.; Chun, Y.; Xu, Q. Preparation of shaped magnesium oxide/carbon catalysts using rice grains. *Appl. Catal. A Gen.* **2013**, *460–461*, 26–35. [[CrossRef](#)]
31. Fraile, J.M.; García-Bordeje, E.; Pires, E.; Roldán, L. New insights into the strength and accessibility of acid sites of sulfonated hydrothermal carbon. *Carbon* **2014**, *77*, 1157–1167. [[CrossRef](#)]
32. NIST X-ray Photoelectron Spectroscopy Database; NIST Standard Reference Database Number 20; National Institute of Standards and Technology: Gaithersburg, MD, USA, 2000. [[CrossRef](#)]
33. Petit, C.; Sereych, M.; Bandoz, T.J. Revisiting the chemistry of graphite oxides and its effect on ammonia adsorption. *J. Mater. Chem.* **2009**, *19*, 9176–9185. [[CrossRef](#)]
34. Takagaki, A.; Toda, M.; Okamura, M.; Kondo, J.N.; Hayashi, S.; Domen, K.; Hara, M. Esterification of higher fatty acids by a novel strong solid acid. *Catal. Today* **2006**, *116*, 157–161. [[CrossRef](#)]
35. Rodrigues, R.; Gonçalves, M.; Mandelli, D.; Pescarmona, P.P.; Carvalho, W.A. Solvent-free conversion of glycerol to Solketal catalysed by activated carbons functionalized with acid groups. *Catal. Sci. Technol.* **2014**, *4*, 2293–2301. [[CrossRef](#)]
36. Kolvari, E.; Koukabi, N.; Hosseini, M.M. Perlite: A cheap natural support for immobilization of sulfonic acid as a heterogeneous solid acid catalyst for the heterocyclic multicomponent reaction. *J. Mol. Catal. A Chem.* **2015**, *397*, 68–75. [[CrossRef](#)]
37. Fraile, J.M.; García-Bordejé, E.; Roldán, L. Deactivation of sulfonated hydrothermal carbons in the presence of alcohols: Evidences for sulfonic esters formation. *J. Catal.* **2012**, *289*, 73–79. [[CrossRef](#)]
38. Santos, E.M.; de Carvalho Teixeira, A.P.; Silva, F.G.; Cibaka, T.E.; Araújo, M.H.; Oliveira, W.X.C.; Medeiros, F.; N. Brasil, A.; de Oliveira, L.S.; Lago, R.M. New heterogeneous catalyst for the esterification of fatty acid produced by surface aromatization/sulfonation of oilseed cake. *Fuel* **2015**, *150*, 408–414. [[CrossRef](#)]
39. Esteban, J.; Ladero, M.; García-Ochoa, F. Kinetic modelling of the solventless synthesis of Solketal with a sulphonic ion exchange resin. *Chem. Eng. J.* **2015**, *269*, 194–202. [[CrossRef](#)]

40. Serafim, H.; Fonseca, I.M.; Ramos, A.M.; Vital, J.; Castanheiro, J.E. Valorization of glycerol into fuel additives over zeolites as catalysts. *Chem. Eng. J.* **2011**, *178*, 291–296. [[CrossRef](#)]
41. Nanda, M.R.; Yuan, Z.; Qin, W.; Ghaziaskar, H.S.; Poirier, M.-A.; Xu, C.C. Catalytic conversion of glycerol to oxygenated fuel additive in a continuous flow reactor: Process optimization. *Fuel* **2014**, *128*, 113–119. [[CrossRef](#)]



© 2019 by the authors. Licensee MDPI, Basel, Switzerland. This article is an open access article distributed under the terms and conditions of the Creative Commons Attribution (CC BY) license (<http://creativecommons.org/licenses/by/4.0/>).